Journal of Mines, Metals and Fuels, *71(8) : 1024-1029; 2023. DOI: 10.18311/jmmf/2023/33537*

Print ISSN : 0022-2755

Journal of Mines, Metals and Fuels

Contents available at: www.informaticsjournals.com/index.php/jmmf

Physical and Optical Properties of Silicon Doped LaOF: Gd^{3+} Nanoparticles Prepared by Combustion Method

A. Jayasheelan[1], R. Venkatesh[2], N. Hanumantharaju[1]*, G. Chandrashekaraiah[3], K. K. Mohankeshava[1], J. Shivakumar[4], P. Shankar[5], V. C. Veeranna Gowda[1], Karanam Madhavi[1] and Wajeeha Sultana[1]

[1]Department of Physics, Maharani's Science College for Women Palace Road, Bangalore – 560001, Karnataka, India; hanu20777@gmail.com
[2]Department of Physics, B.M.S. Instutite of Technology, Bangalore – 560064, Karnataka, India
[3]Department of Physics, Government First College, Kunigal – 572130, Karnataka, India
[4]Department of Physics, Government College, Gubbi – 572216 Karnataka, India
[5]Department of Physics, Sai Vidya Institute of Technology, Bangalore – 560064, Karnataka, India

Abstract

The bandgap energy and density of the sample were found by the analytical method. The density was found to increase up to 5 mol%, depicting the compactness of the sample and then decreasing with gadolinium content. Molar volume (Vm), Gd^{3+} ion concentration (N), refractive index (n), electronic polarizability (α_e), reflection loss (R_L), polaron radius (r_p), internuclear distance (r_i), field strength(F), dielectric constant(ε) of the sample were calculated.

Keywords: *Combustion, Gd^{3+}, LaOF, Optical, Physical, Rare Earth, Silicon*

1.0 Introduction

In recent days, increasing the development of the white Light-Emitting Diode (LED) industry, rare earth (Gd^{3+}) ion-activated lanthanum oxyfluoride inorganic luminescent phosphor materials have been diverse applications in potential fields over the earlier decades, such as White Light Emitting Diodes (WLEDs), cathode ray tubes, plasma display panels, photovoltaic cells, fluorescent bulbs, lasers, optical sensors and innumerable energy storage appliances[1-5]. Amongst all the progressive applications of inorganic Nano Phosphors (NPs), WLEDs have been considered for future solid-state lighting resources due to their favorable properties, such as enriched brightness, eco-friendliness, regulatable emission, improved physical, chemical and thermal stability, long lasting strengths, less power consumption etc. Presently, in the market, commercially available W-LEDs with a blue InGaN chip in combination with a yellow phosphor (YAG:Ce^{3+})[6] and a group of red, green, and blue phosphors containing Near ultraviolet (N-UV) LED chips were non-existence of red, green constituent and less color representation index. In this regard, the discovery of novel red, green and blue phosphors-converted light-emitting diodes LEDs (pc-LEDs) is paying attention to increasing the prospects for tunable emission through the phosphors transmission and accessibility of simple approaches for both materials design and production of WLEDs[7].

We report for the first time the utilization of optimized C-S composite SiO_2@ LaOF: Gd^{3+} NPs as a distinctive fluorescent label for the identification of LFPs. For the visualization of LFPs these fluorescent NPs are successful on various surfaces, such as magazine covers, playing

**Author for correspondence*

cards, metallic scales, aluminium foil, and different types of fruits and vegetables. Initially, SiO_2 C-S NPs were synthesized by Stöber method. Later, SiO_2@ LaOF: Eu^{3+}, Li^+ NP coat was developed on SiO_2 by solution combustion method, and all the samples were well characterized to study the physical and optical properties.

2.0 Experimental

The LaOF: Gd^{3+} NPs were fabricated using the solution combustion method, and all the chemicals used were of analytical grade with 99.9% purity (Sigma Aldrich). According to stoichiometric calculation, Lanthanum nitrate [$La(NO_3)_3.6H_2O$], Ammonium fluoride [NH4F] and Gadolinium nitrate [$Gd(NO_3.6H_2O$] were used as starting materials and EGCG extract as a fuel. These mixtures were run through deionized water in a Petri dish and make a homogeneous mixture by using a magnetic stirrer for ~20 min. This clear solution was kept in a preheated muffle furnace (500 ± 10 ^{0}C). The solution changed into lotion and then became burned. The final product was calcinated for 2 h at ~ 800 ^{0}C. The schematic illustration for the synthesis of LaOF: Gd^{3+} NPs.

3.0 Results and Discussion

3.1 Density and Molar Volume

The density of the LaOF sample was found using Archimedes Principle. Acetone (0.786 g/cm^3) was used as an immersion liquid for the sample to measure its density. The sample density was calculated using the relation.

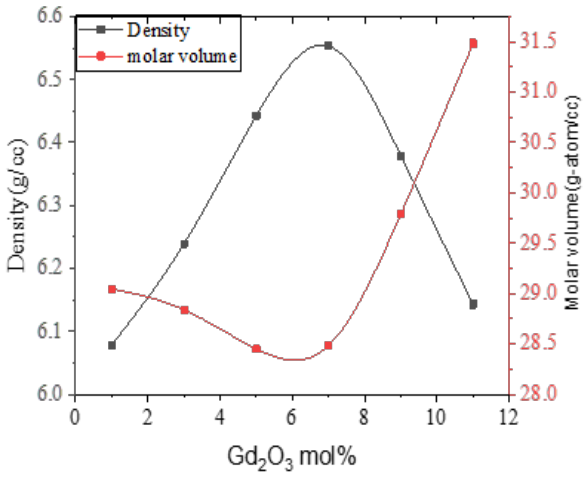

Figure 1. Variation of density and molar volume with Gd_2O_3 content.

$$\rho_{glass} = \frac{W_A}{W_A - W_B} 0.786 \quad (g/cm^3)$$

where, W_A is the weight of the sample in air and W_B is the weight of the sample in acetone. The measurement was repeated three times for each sample to approximate the average value. The values are listed in Table 1.

The density for the sample increases, and the corresponding molar volume decreases up to 7 mol% gadolinium content due to bridging oxygen atoms and then finds the opposite nature beyond 7 mol% as shown in Figure 1 due to non-bridging oxygen atoms. The non-linear variation of density, molar volume and Oxygen

Table 1. Density (ρ), Molar volume (V_m) and Oxygen Packing Density (OPD) with Gd_2O_3 mol%

Phosphor	Density (g/cc)	Molar volume (x 10^{-5} m^3)	OPD (g-atom/litre)
LaOF:Gd^{3+} (1 mol%)	6.078	29.080	35.075
LaOF:Gd^{3+} (3 mol%)	6.239	28.932	36.636
LaOF:Gd^{3+} (5 mol%)	6.442	28.601	38.459
LaOF:Gd^{3+} (7 mol%)	6.553	28.691	39.733
LaOF:Gd^{3+} (9 mol%)	6.378	30.063	39.250
LaOF:Gd^{3+} (11 mol%)	6.143	31.829	38.329

Packing Density (OPD) with Gd^{3+} concentration is due to the electronic and ionic hopping mechanism in the network[8].

3.2 Physical and Optical Properties

Gd^{3+} ion concentration(N), density (ρ) and refractive index(n) were used to estimate the physical and optical properties of the samples, such as electronic polarizability (α_e), reflection loss (R_L), polaron radius (r_p), inter nuclear distance (r_i), field strength(F) and dielectric constant (ε) using the standard relations and the obtained values are listed in Table 2.

3.2.1 Ion Concentration (N)

Gadolinium ion concentration () can be calculated using the relation[9]

$$N = \frac{(Avogadro's\ number)\ (glass\ density)}{(glass\ average\ molecular\ weight)}\ (\%\ of\ RE)$$

The concentration of Gd^{3+} ions increases in the sample with the percentage of Gd^{3+} ions. Because of ratifying the compactness of the system with the addition of gadolinium oxide, the polaron radius and inter nuclear distance has been calculated using the below relations[10].

Polaron radius, $r_p = \left(\frac{1}{2}\right)\left(\frac{\pi}{6N}\right)^{1/3}$

Inter nuclear distance, $r_i = \left(\frac{1}{N}\right)^{1/3}$

where, N indicates Gd^{3+} ion concentration. Table 2 depicts a decrease in inter nuclear distance and polaron radius with Gd^{3+} ion concentration. This result leads to the Gd-O bond strength increases, which enables the strong field near the Gd^{3+} ions.

The compactness of the sample shows that the degree of delocalization of electrons decreases, which results in a decrease in band gap energy[11,12].

3.2.2 Field Strength (F)

Field strength gives information about the arrangement of ions in the sample the values were calculated using the relation given[10] and were presented in Table 2.

Field strength, $F = \left(\frac{z}{r_p^2}\right)$

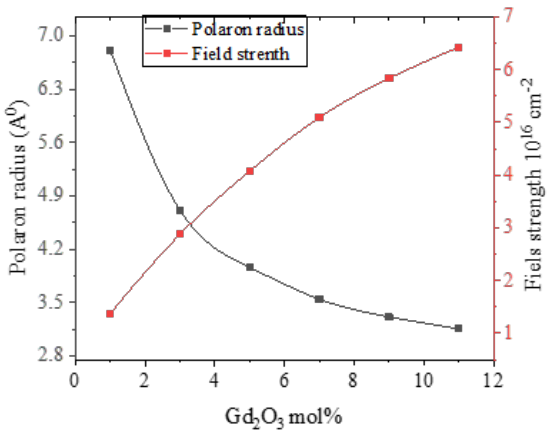

Figure 2. Variation of polaron radius and filed strength with Gd_2O_3 mol%.

where, Z is the atomic mass of gadolinium oxide and r_p is the polaron radius.

The obtained values show the rigidity of the sample increases with Gd^{3+} content. The variation of polaron radius and field strength with Gd_2O_3 content is shown in Figure 2. This figure shows field strength increases while polaron radius decreases. In general, field strength and polaron radius shows the opposite behavior and which is observed in our study.

3.2.3 Refractive Index and Electronic Polarizability

When light interacts with atoms of the sample, the parameter refractive index can be calculated, and this parameter depends on cation polarizability and density. The electronic polarizability (α_m) is used in the field of applications like optical and electronic devices[13]. Due to the application of the electromagnetic field, the electronic polarizability exhibits distortion in the electronic cloud[14]. The parameter α_m was measured using the Clausius-Mosotti equation

$$\alpha_m = \left(\frac{3}{4\pi N_A}\right) R_m$$

where, R_m is the molar refraction and N_A is Avogadro's number

The molar refraction $R_m = \left(\frac{n^2-1}{n^2+2}\right) V_m$

where, V_m is the molar volume, and n is the refractive index

The variation of refractive index and electronic polarizability is shown in Figure 3. From the figure the increasing values may be due to increasing in Gd^{3+} ion content, which has high electronic polarizability (7.432 $(A^0)^3$) than B^{3+} (0.002 $(A^0)^3$)[15,16].

3.3.5 Metallization Criterion(M)

The metallic and non-metallic nature of the sample was based on metallization criterion values[17]. The metallization criterion of the sample can be calculated using the relation given below

$$M = 1 - \frac{R_m}{V_m}$$

where, R_m is molar refraction and V_m molar volume.

If the value $R_m/V_m < 1$, the sample is non-metallic and if the value $R_m/V_m > 1$, the sample is metallic. It is established that from the above equation, the sample is non-metallic, and the calculated values are listed in Table 2. The highest value of the metallization criterion (0.454) calculated for the lanthanum oxyfluoride discloses that lanthanum-ion reveals the highest band gap energy and insulating nature in the sample, which is confirmed by the band gap energy values. Larger metallization criterion values depict that width of both conduction and valence bands reduces, which intern shows a wider optical band gap energy[18].

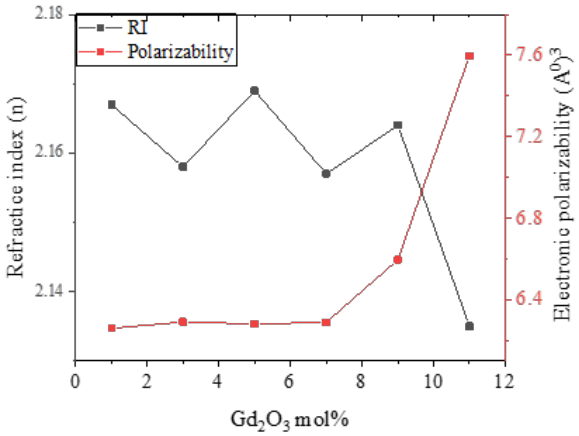

Figure 3. Variation of refractive index and electronic polarizability with Gd_2O_3 content.

3.3.6 Optical Band Gap Energy

The optical band gap energy for the sample is calculated using Davis and Mott theory[19]. Optical transitions and electronic band structures were explained because of the absorption effect, which could be able to elaborate the optical band gap energy[20]. The absorption coefficient α(ϑ) is a function of photon energy for indirect and direct band gap energy.

$$\alpha = \alpha_0(h\vartheta - E_g)^n/h\vartheta$$

Table 2. The physical and optical properties of **LaOF:Gd^{3+} NPs**

Physical and optical properties	LaOF:Gd^{3+} nanophosphors					
	1 mol %	3 mol %	5 mol %	7 mol %	9 mol %	11 mol %
Gd^{3+} concentration (x 10^{20} ion/cm^3)	2.071	6.2452	10.529	14.695	18.031	20.815
Polaron radius (r_p)(A')	6.81	4.714	3.961	3.544	3.311	3.156
Inter nuclear distance (r) (A')	16.902	11.699	9.829	8.796	8.216	7.832
Field Strength (F)(x10^{16} cm^{-2})	1.3 8	2.88	4.078	5.095	5.839	6.426
Refractive Index (n)	2.167	2.142	2.169	2.157	2.164	2.135
Reflection loss R %	0.135	0.132	0.136	0.134	0.135	0.131
Dielectric constant (ε)	4.697	4.589	4.708	4.655	4.683	4.562
Optical dielectric constant (dpt/dp)	3.697	3.589	3.708	3.655	3.683	3.562
Molar Refraction (R_M) (cm^{-3})	16.053	15.759	15.81	15.759	16.568	17.278
Metallization criterion	0.447	0.455	0.447	0.45	0.448	0.457
Electronic polarizability (α_m) $(A')^3$	6.26	6.291	6.282	6.289	6.597	7.597
OPD (g-atom/litre)	35.075	36.636	38.459	39.732	39.25	38.329

where, E_g optical band gap energy, α_0 is energy independent constant and n is the exponent. If the exponent n=1/2 and 2 represents the allowed direct and indirect transition. It is found that band gap energy (E_g) values decrease up to 7mol% of Gd_2O_3 content and then increase as shown in Figure 4, the values are listed in Table 1.

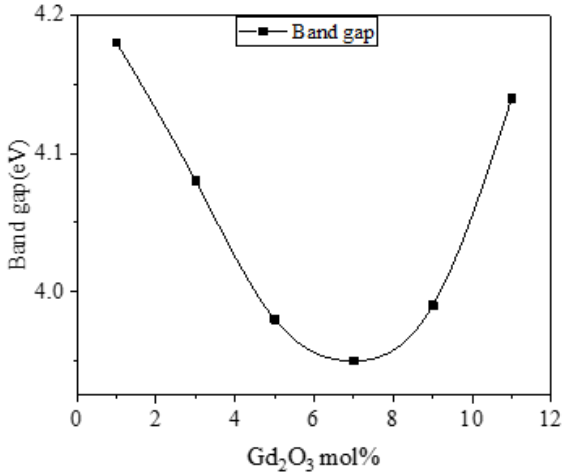

Figure 4. Variation of band gap with Gd_2O_3 content.

4.0 Conclusion

The LaOF: Gd^{3+} NPs were fabricated using the solution combustion method and estimated the physical and optical properties. The density of the samples found non-linear variation due to the bridging and non-bridging of oxygen atoms, which shows the stiffness and rigidity of the samples. The concentration of Gd^{3+} ions increases in the sample with the percentage of Gd^{3+} ions. Because of ratifying the compactness of the system with the addition of gadolinium oxide, the polaron radius and inter nuclear distance has been calculated, and we found that field strength increases while polaron radius decreases.

5.0 Acknowledgment

The authors are thankful to Dr. Sriprakash G, Professor, Department of Physics, for his fruitful discussion in writing the paper and Maharani Cluster University, Bangalore.

6.0 References

1. Evanics F, Diamente PR, van Veggel FCJM, Stanisz GJ, Prosser RS. Water-soluble GdF3 and GdF3/LaF3 nanoparticles physical characterization and NMR relaxation properties. ACS Applied Engineering Materials. 2006; 18(10):2499–505. https://doi.org/10.1021/cm052299w
2. Wegh RT, Donker H, Oskam KD, Meijerink A. Visible quantum cutting in Eu^{3+}-doped gadolinium fluorides via downconversion. Journal of Luminescence. 1999; 82(2):93–104. https://doi.org/10.1016/S0022-2313(99)00042-3
3. Fujihara S, Koji S, Kimura T. Structure and optical properties of (Gd,Eu)F3-nanocrystallized sol-gel silica films. Journal of Materials Chemistry. 2004; 14(8):1331–35. https://doi.org/10.1039/B313784H
4. Pi D, Wang F, Fan X, Wang M. Luminescence behavior of Eu^{3+} doped LaF3 nanoparticles, spectrochim. Spectrochimica Acta, Part A: Molecular and Biomolecular Spectroscopy. 2005; 61(11-12):2455–9. https://doi.org/10.1016/j.saa.2004.09.009
5. Zhang H, Li H, Li D. Synthesis and characterization of ultrafine CeF3 nanoparticles modified by catanionic surfactant via a reverse micelles route. Journal of Colloid and Interface Science. 2006; 302(2):509–15. https://doi.org/10.1016/j.jcis.2006.06.062
6. Sudarsan V, Sivakumar S, Raudsepp M. General and convenient method for making highly luminescent sol–gel derived silica and alumina films by using LaF3 nanoparticles doped with lanthanide ions (Er^{3+}, Nd^{3+}, and Ho^{3+}). Chemistry of Materials. 2005; 17(18):4736–42. https://doi.org/10.1021/cm051065+
7. Lezhnina MM, Kaetker H, Kynast UH. Synthesis and optical characterization of rare earth nanofluorides. Optical Materials. 2007; 30(2):264-72. https://doi.org/10.1016/j.optmat.2007.03.014
8. Raju NH. Role of MnO_2 on optical , physical and thermal properties in sodium zinc phosphate glasses. International Journal of Research and Analytical Reviews. 2019; 6(1):542-548.
9. Tan CZ, Arndt J. The mean polarizability and density of glasses. Physica B: Condensed Matter. 1997; 229(3-4):217-24. https://doi.org/10.1016/S0921-4526(96)01032-0
10. Pawar PP, Munishwar SR, Gedam RS. Eu_2O_3 doped bright orange-red luminescent lithium alumino-borate glasses for solid state lighting. Journal of Luminescence. 2018; 200:216–24. https://doi.org/10.1016/j.jlumin.2018.04.026
11. Ramteke DD, Gedam RS. Luminescence properties of Gd^{3+} containing glasses for Ultra-Violet (UV) light.

Journal of Rare Earths. 2014; 32(5):389–93. https://doi.org/10.1016/S1002-0721(14)60082-X

12. Marzouk MA, Ouis MA, Hamdy YM. Spectroscopic studies and luminescence spectra of Dy_2O_3 doped lead phosphate glasses. Silicon. 2012; 4:221–7. https://doi.org/10.1007/s12633-012-9125-z
13. Cha YJ, Kim JH, Yoon J, Lee BS, Choi S, Hong KS, *et al*. Synthesis, electronic polarizability and β -BaB_2 O_4 crystallization in BaO - B_2O_3 - TeO_2 glasses. Journal of Non-Crystalline Solids. 2015; 429:143–7. https://doi.org/10.1016/j.jnoncrysol.2015.09.010
14. Komatsu T, Ito N, Honma T, Dimitrov V. Temperature dependence of refractive index and electronic polarizability of RO e TeO_2 glasses (R¼ Mg , Ba , Zn). Solid State Sciences. 2012; 14(10):1419–25. https://doi.org/10.1016/j.solidstatesciences.2012.08.005
15. Dimitrov V, Komatsu T. Optical basicity and single bond strength of oxide glasses. Journal of Chemical Technology and Metallurgy. 2013; 48:549–54.
16. Narayanan MK, Shashikala HD. Physical, mechanical and structural properties of BaO-CaF_2-P_2O_5 glasses. Journal of Non-Crystalline Solids. 2015; 430:79-86. https://doi.org/10.1016/j.jnoncrysol.2015.10.006
17. Alazoumi SH, Aziz SA, El-Mallawany R, Aliyu US, Kamari HM, Zaid MHMM, *et al*. Optical properties of zinc lead tellurite glasses. Results in Physics. 2018; 9:1371–6. https://doi.org/10.1016/j.rinp.2018.04.041
18. Jiang C, Wang X, Zhu Q, Nie Q, Zhang X. Improvements on the optical properties of Ge-Sb-Se chalcogenide glasses with iodine incorporation. Infrared Physics and Technology. 2015; 73:54–61. https://doi.org/10.1016/j.infrared.2015.09.001
19. Davis EA, Mott NF. Conduction in non-crystalline systems V. Conductivity, optical absorption and photoconductivity in amorphous semiconductors. The Philosophical Magazine. 1970; 22(179):903–22. https://doi.org/10.1080/14786437008221061
20. Urbach F. The long-wavelength edge of photographic sensitivity and of the electronic absorption of solids. Physical Review Letters. 193; 92. https://doi.org/10.1103/PhysRev.92.1324